

Supplementary material

On the effect of metal loading on the performance of Co catalysts supported on mixed MgO–La₂O₃ oxides for ammonia synthesis

Hubert Ronduda ^a, Magdalena Zybert ^a, Wojciech Patkowski ^a, Kamil Sobczak ^b, Dariusz Moszyński ^c, Aleksander Albrecht ^c, Adam Sarnecki ^c, and Wioletta Raróg-Pilecka ^{a*}

^a Warsaw University of Technology, Faculty of Chemistry, Noakowskiego 3, 00-664 Warsaw, Poland

^b University of Warsaw Biological and Chemical Research Centre, Żwirki i Wigury 101, 02-089 Warsaw, Poland

^c West Pomeranian University of Technology in Szczecin, Faculty of Chemical Technology and Engineering, 42 Piastów Ave, 71-065 Szczecin, Poland

*Corresponding author

e-mail: wiola@ch.pw.edu.pl

tel. +48 22 234 57 66

Number of pages: 9

Number of figures: 12

Number of tables: 2

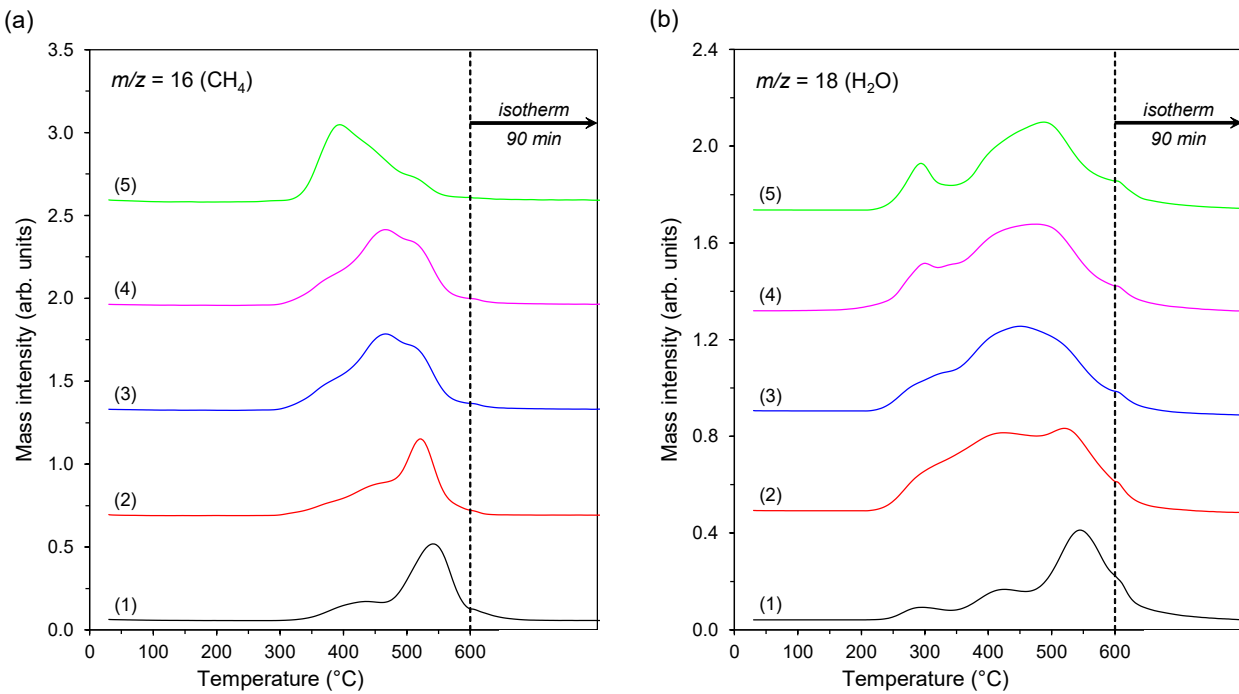


Figure S1. Evolution profiles of (a) CH_4 and (b) H_2O during hydrogen temperature-programmed reduction ($\text{H}_2\text{-TPR}$) of the Co catalyst precursors with different Co loadings: (1) $\text{Co}(10)/\text{Mg-La}$, (2) $\text{Co}(20)/\text{Mg-La}$, (3) $\text{Co}(30)/\text{Mg-La}$, (4) $\text{Co}(40)/\text{Mg-La}$, and (5) $\text{Co}(50)/\text{Mg-La}$.

The $\text{H}_2\text{-TPR}$ profiles of the Co catalyst precursors indicated that the formation of CH_4 and H_2O was completed at a temperature of about 600 °C. The mass signal of $m/z = 16$ indicated the presence of methane, which was due to the decomposition of lanthanum dioxide carbonate, accompanied by the formation of methane [1]. The mass signal of $m/z = 18$ indicated the presence of water, which was due to the reduction of Co oxide species to metallic Co and the methanation of CO_2 [1].

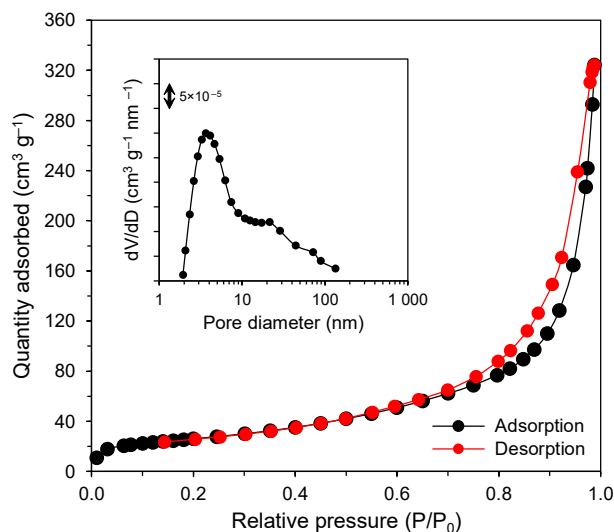


Figure S2. Nitrogen adsorption-desorption isotherm of the Mg-La support. The inset shows the corresponding BJH pore size distribution curve. The nitrogen adsorption-desorption isotherm was obtained from the ASAP 2020 analyser, and the surface area was calculated by Brunauer–Emmett–Teller (BET) method, pore size distribution and pore volume were estimated by Barrett–Joyner–Halenda (BJH) method.

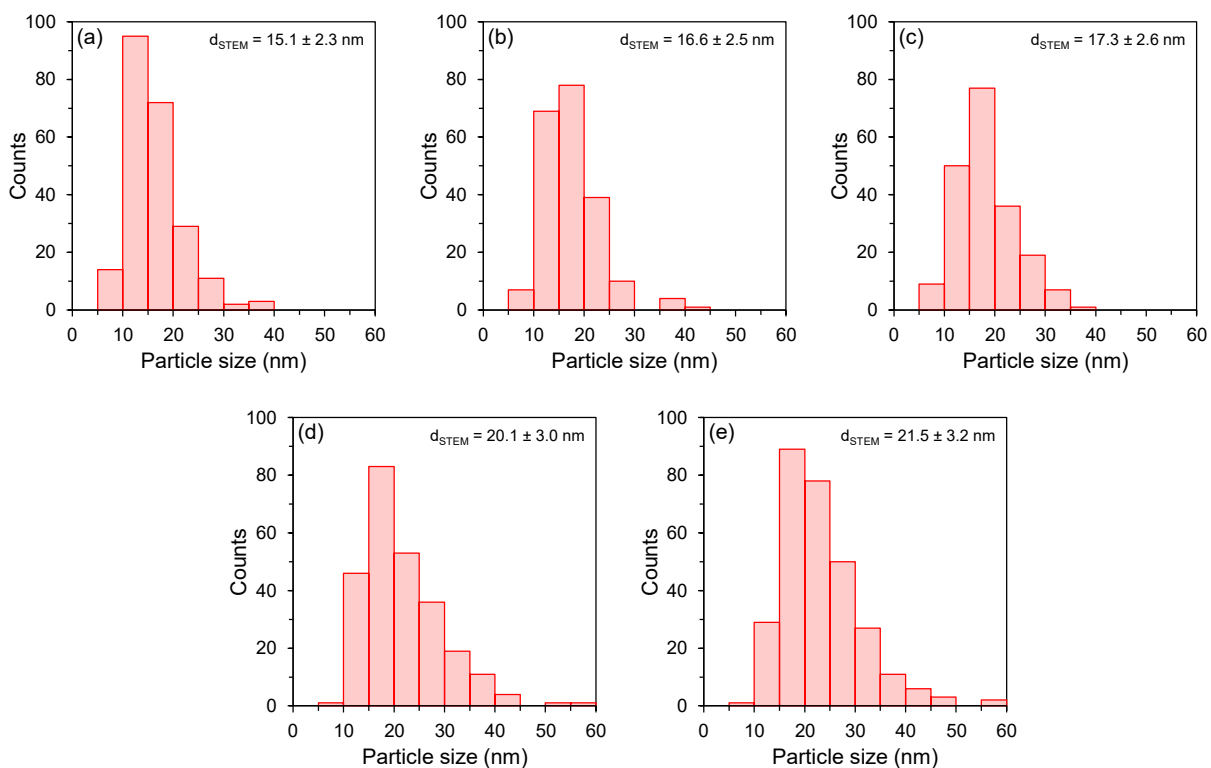


Figure S3. Co particle size distributions obtained from STEM-EDX images of the Co catalysts with different Co loadings: (a) Co(10)/Mg-La, (b) Co(20)/Mg-La, (c) Co(30)/Mg-La, (d) Co(40)/Mg-La, and (e) Co(50)/Mg-La.

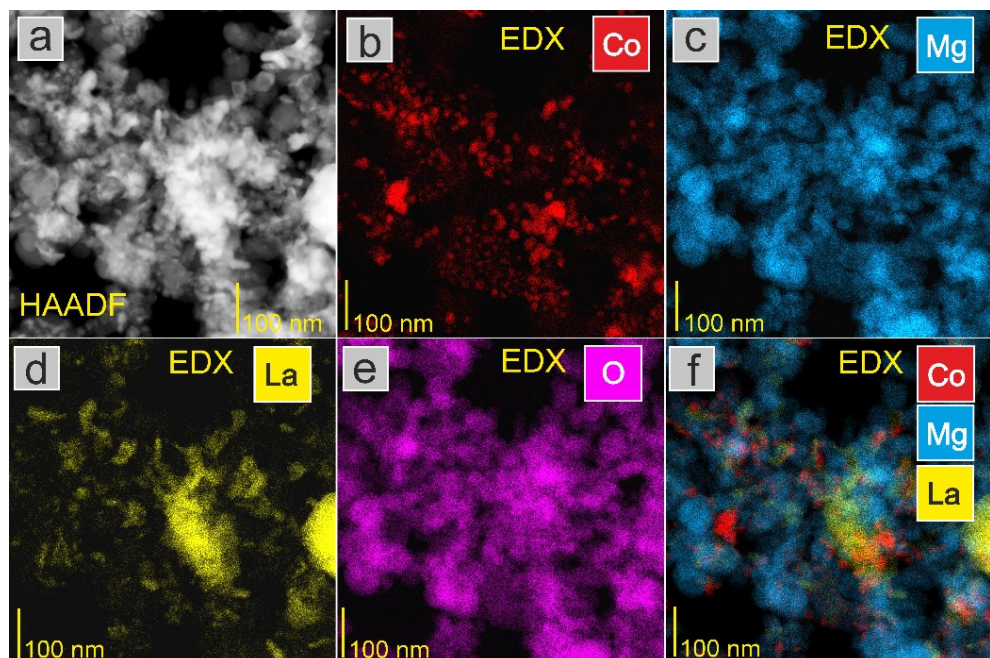


Figure S4. (a) HAADF-STEM image of Co(10)/Mg-La catalyst and corresponding EDX distribution maps of (b) Co-K, (c) Mg-K, (d) La-L, (e) O-K, and (f) reconstructed overlay image of Co, Mg, and La.

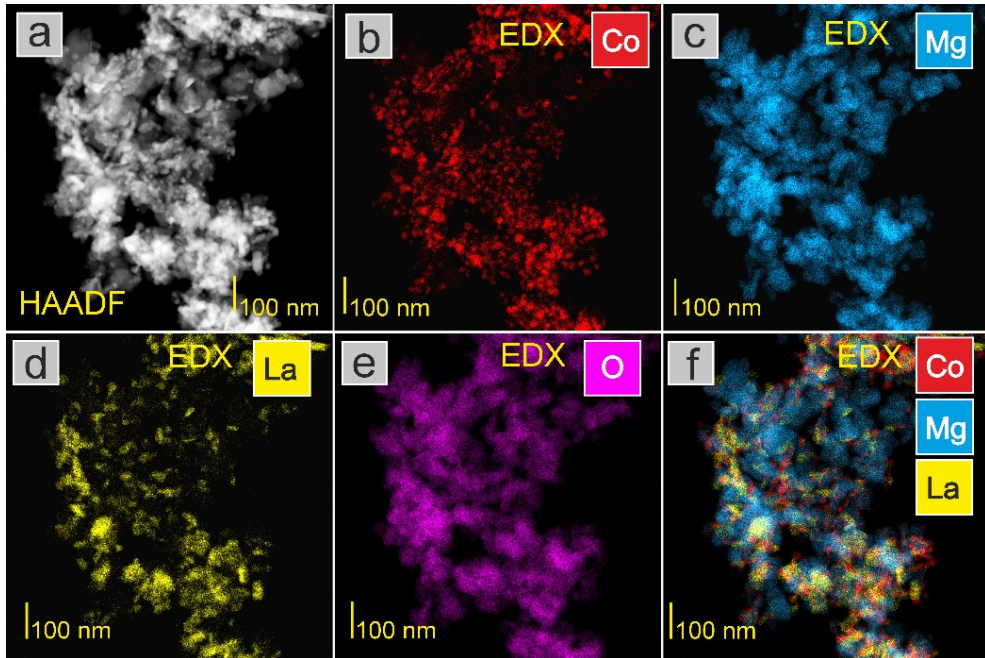


Figure S5. (a) HAADF-STEM image of Co(20)/Mg-La catalyst and corresponding EDX distribution maps of (b) Co-K, (c) Mg-K, (d) La-L, (e) O-K, and (f) reconstructed overlay image of Co, Mg, and La.

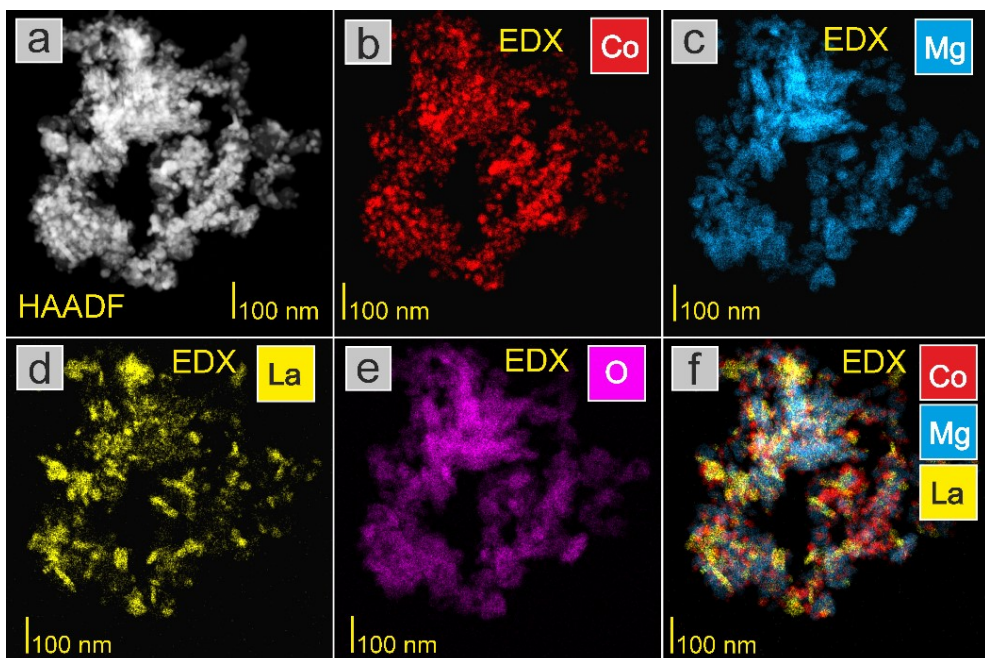


Figure S6. (a) HAADF-STEM image Co(30)/Mg-La catalyst and corresponding EDX distribution maps of (b) Co-K, (c) Mg-K, (d) La-L, (e) O-K, and (f) reconstructed overlay image of Co, Mg, and La.

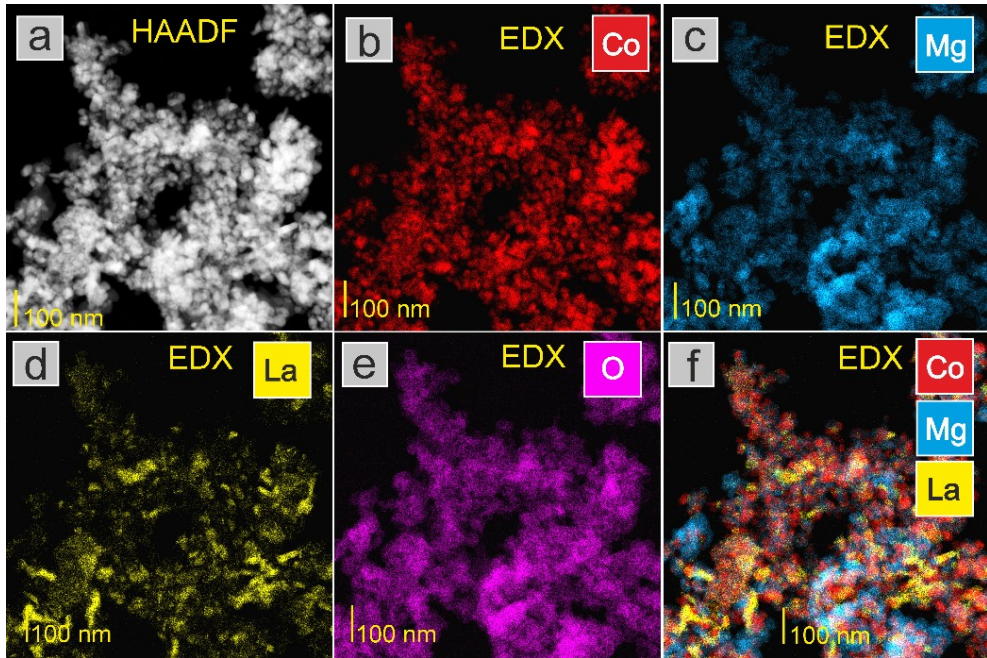


Figure S7. (a) HAADF-STEM image of Co(40)/Mg-La catalyst and corresponding EDX distribution maps of (b) Co-K, (c) Mg-K, (d) La-L, (e) O-K, and (f) reconstructed overlay image of Co, Mg, and La.

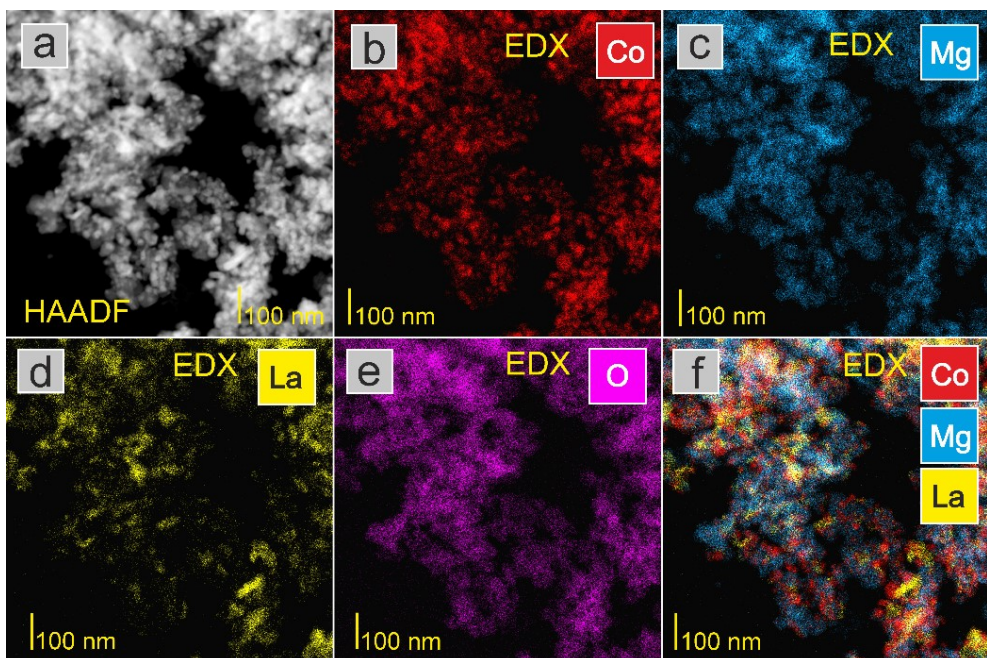


Figure S8. (a) HAADF-STEM image of Co(50)/Mg-La catalyst and corresponding EDX distribution maps of (b) Co-K, (c) Mg-K, (d) La-L, (e) O-K, and (f) reconstructed overlay image of Co, Mg, and La.

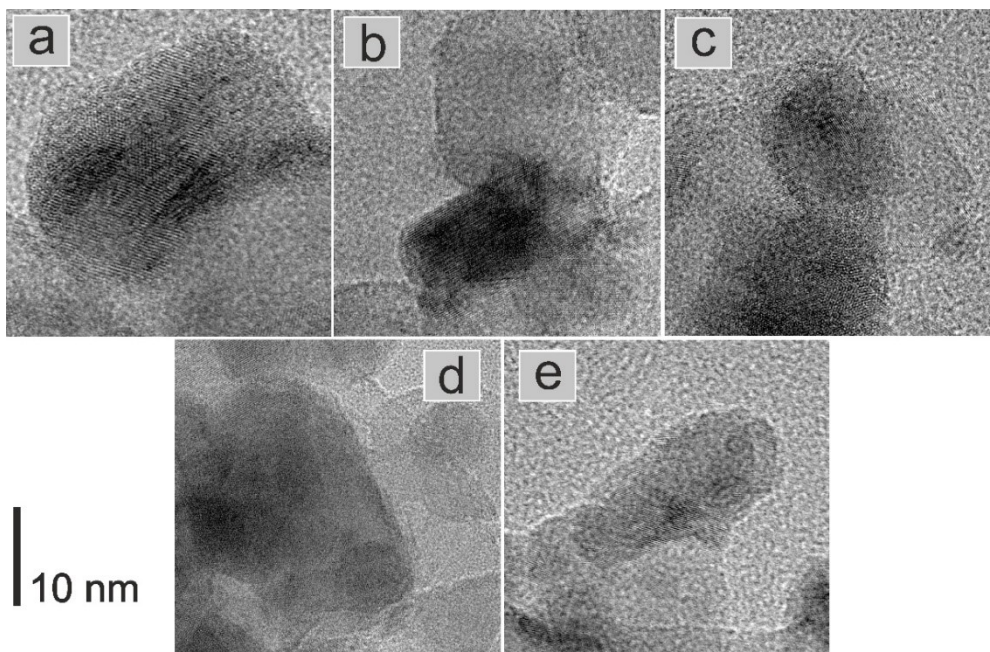


Figure S9. TEM images of the Co catalysts with different Co loadings: (a) Co(10)/Mg–La, (b) Co(20)/Mg–La, (c) Co(30)/Mg–La, (d) Co(40)/Mg–La, and (e) Co(50)/Mg–La.

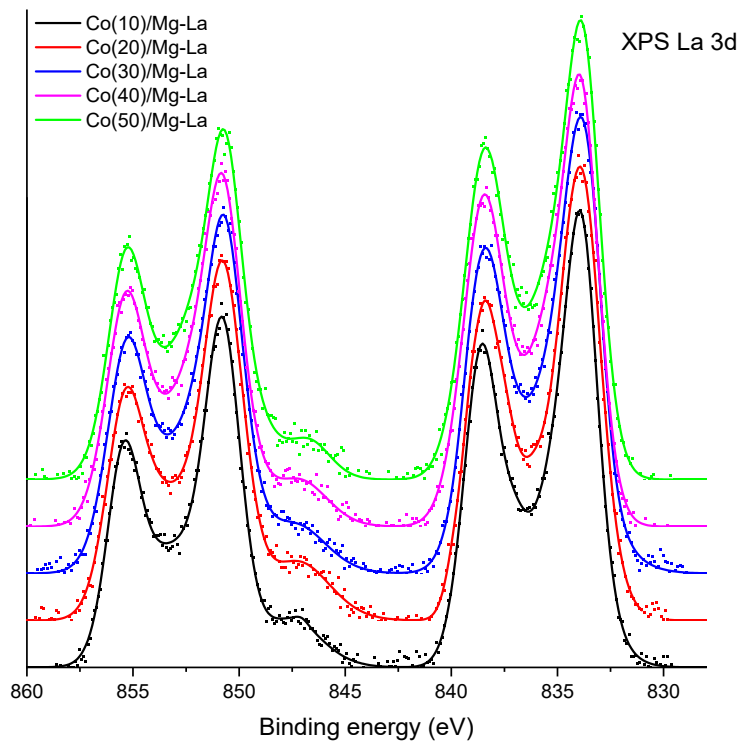


Figure S10. XPS La 3d spectra of the Co catalysts with different Co loadings.

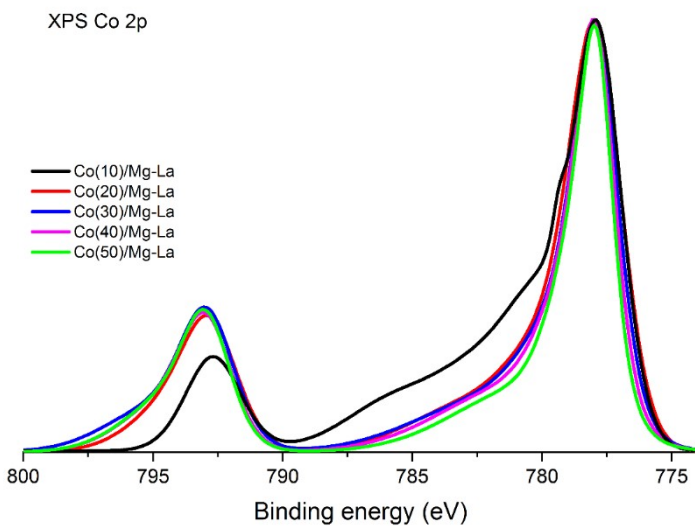


Figure S11. XPS Co 2p spectra of the Co catalysts with different Co loadings.

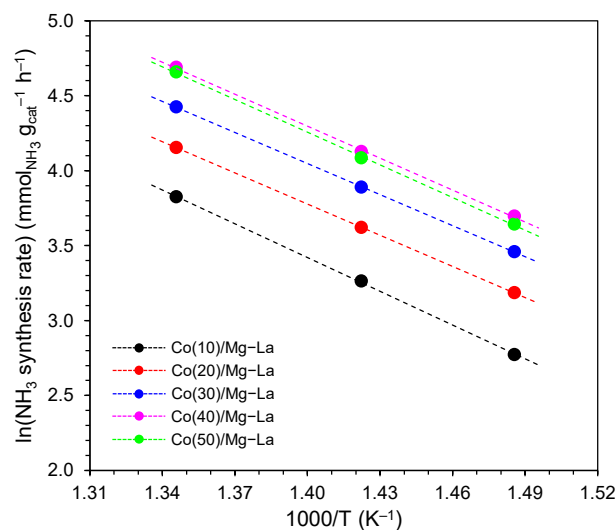


Figure S12. Arrhenius plots for the rate of ammonia synthesis at 6.3 MPa over the Co catalysts with different Co loadings.

Table S1. Composition of the Co catalysts obtained by ICP-AES.

Entry	Catalyst	Chemical composition (wt%)		
		Co	Mg	La
1	Co(10)/Mg-La	10.6	38.1	28.1
2	Co(20)/Mg-La	21.2	34.1	24.9
3	Co(30)/Mg-La	30.7	28.9	19.9
4	Co(40)/Mg-La	41.1	24.4	16.6
5	Co(50)/Mg-La	50.4	20.7	15.1

Table S2. Comparison of the catalytic performance for NH₃ synthesis of different catalysts.

Entry	Catalyst	Metal ^a	Promoter ^a	Reaction temperature (°C)	Reaction pressure (MPa)	Gas hourly space velocity ^b (mL g _{cat} ⁻¹ h ⁻¹)	NH ₃ synthesis rate ^c (mmol _{NH₃} g _{cat} ⁻¹ h ⁻¹)	Reference
1	Ba-Ru-Li/AC	Ru (5 wt%)	Li (8 wt%) + Ba (5 wt%)	459	3	62400	106	[2]
2	Ru/MgO	Ru (4 wt%)	—	400	5	—	7	[3]
3	Ru/BaTiO ₃	Ru (4 wt%)	—	400	5	—	16	[3]
4	Ru/CeO ₂	Ru (4 wt%)	—	400	5	—	9	[3]
5	Ru/CeO ₂ -r	Ru (10 wt%)	—	400	10	233300	115	[4]
6	Ru/La ₂ Ce ₂ O ₇	Ru (4 wt%)	—	425	10	—	53	[5]
7	Fe _{1-x} O	Fe (70 wt%)	Al + Ca + K (<10 wt%)	430	3	7200	12	[6]
8	Fe ₃ O ₄	Fe (70 wt%)	Al + Ca + K (<10 wt%)	430	3	7200	9	[6]
9	FeOOH-K/Al ₂ O ₃	Fe (22 wt%)	K (5 wt%)	500	9	12000	29	[7]
10	2%Cs-FePc	Fe (19 wt%)	Cs (2 wt%)	400	7	12000	20	[8]
11	10%Cs-FePc	Fe (19 wt%)	Cs (10 wt%)	400	7	12000	26	[8]
12	Fe _{1-x} O (ZA-5)	Fe	Al + Ca + K + ...	400	10	10000	19	[9,10]
13	Co/Ba	Co (73 wt%)	Ba (12 wt%)	400	6.3	170300	51	[11]
14	Co/La/Ba	Co (59 wt%)	Ba (11 wt%) + La (7 wt%)	400	6.3	137700	76	[11]
15	Co/CeO ₂ -H	Co (7 wt%)	—	400	10	240000	35	[12]
16	Co/CeO ₂	Co (6 wt%)	—	400	10	—	12	[13]
17	Ba-Co/CeO ₂	Co (6 wt%)	Ba (3 wt%)	400	10	—	15	[13]
18	K-Co/CeO ₂	Co (6 wt%)	K (9 wt%)	400	10	—	3	[13]
19	Co(10)/Mg-La	Co (10 wt%)	—	400	6.3	140000	16	This work
20	Co(20)/Mg-La	Co (20 wt%)	—	400	6.3	140000	24	This work
21	Co(30)/Mg-La	Co (30 wt%)	—	400	6.3	140000	32	This work
22	Co(40)/Mg-La	Co (40 wt%)	—	400	6.3	140000	40	This work
23	Co(50)/Mg-La	Co (50 wt%)	—	400	6.3	140000	38	This work

^a Rounded to the nearest 1 wt%. ^b Rounded to the nearest 100 mL g_{cat}⁻¹ h⁻¹. ^c Rounded to the nearest 1 mmol_{NH₃} g_{cat}⁻¹ h⁻¹

References

- [1] H. Ronduda, M. Zybert, W. Patkowski, A. Ostrowski, P. Jodłowski, D. Szymański, W. Raróg-Pilecka, Co supported on Mg–La mixed oxides as an efficient catalyst for ammonia synthesis, *Int. J. Hydrogen Energy*, 2022, **47**, 35689–35700. <https://doi.org/10.1016/j.ijhydene.2022.08.144>
- [2] J. Zheng, F. Liao, S. Wu, G. Jones, T.-Y. Chen, J. Fellowes, T. Sudmeier, I.J. McPherson, I. Wilkinson, S.C.E. Tsang, Efficient Non-dissociative Activation of Dinitrogen to Ammonia over Lithium-Promoted Ruthenium Nanoparticles at Low Pressure, *Angew. Chem. Int. Ed.*, 2019, **58**, 17335–17341. <https://doi.org/10.1002/anie.201907171>
- [3] Z. Wang, J. Lin, R. Wang, K. Wei, Ammonia synthesis over ruthenium catalyst supported on perovskite type BaTiO₃, *Catal. Commun.*, 2013, **32**, 11–14. <https://doi.org/10.1016/j.catcom.2012.11.024>
- [4] B. Lin, Y. Liu, L. Heng, X. Wang, J. Ni, J. Lin, L. Jiang, Morphology Effect of Ceria on the Catalytic Performances of Ru/CeO₂ Catalysts for Ammonia Synthesis, *Ind. Eng. Chem. Res.*, 2018, **57**, 9127–9135. <https://doi.org/10.1021/acs.iecr.8b02126>
- [5] W. Han, Z. Li, H. Liu, La₂Ce₂O₇ supported ruthenium as a robust catalyst for ammonia synthesis, *J. Rare Earths*, 2019, **37**, 492–499. <https://doi.org/10.1016/j.jre.2018.09.010>
- [6] A. Jafari, A. Ebadi, S. Sahebdefar, Effect of iron oxide precursor on the properties and ammonia synthesis activity of fused iron catalysts, *Reac. Kinet. Mech. Cat.*, 2019, **126**, 307–325. <https://doi.org/10.1007/s11144-018-1498-6>
- [7] H. Fan, X. Huang, K. Kähler, J. Folke, F. Girgsdies, D. Teschner, Y. Ding, K. Hermann, R. Schlögl, E. Frei, In-Situ Formation of Fe Nanoparticles from FeOOH Nanosheets on γ-Al₂O₃ as Efficient Catalysts for Ammonia Synthesis, *ACS Sustainable Chem Eng.*, 2017, **5**, 10900–10909. <https://doi.org/10.1021/acssuschemeng.7b02812>
- [8] N. Morlanés, W. Almaksoud, R.K. Rai, S. Ould-Chikh, M.M. Ali, B. Vidjayacoumar, B.E. Al-Sabban, K. Albahily, J.-M. Basset, Development of catalysts for ammonia synthesis based on metal phthalocyanine materials, *Catal. Sci. Technol.*, 2020, **10**, 844–852. <https://doi.org/10.1039/C9CY02326G>
- [9] M. Zybert, M. Karasińska, E. Truszkiewicz, B. Mierzwa, W. Raróg-Pilecka, Properties and activity of the cobalt catalysts for NH₃ synthesis obtained by co-precipitation – the effect of lanthanum addition, *Pol. J. Chem. Technol.*, 2015, **17**, 138–143. <https://doi.org/10.1515/pjct-2015-0020>
- [10] Y. Zhou, Y. Ma, G. Lan, H. Tang, W. Han, H. Liu, Y. Li, A highly stable and active mesoporous ruthenium catalyst for ammonia synthesis prepared by a RuCl₃/SiO₂-templated approach, *Chin. J. Catal.*, 2019, **40**, 114–123. [https://doi.org/10.1016/S1872-2067\(18\)63192-4](https://doi.org/10.1016/S1872-2067(18)63192-4)
- [11] H. Liu, *Ammonia Synthesis Catalysts: Innovation and Practice*, World Scientific, 2013.
- [12] B. Lin, Y. Qi, K. Wei, J. Lin, Effect of pretreatment on ceria-supported cobalt catalyst for ammonia synthesis, *RSC Adv.*, 2014, **4**, 38093–38102. <https://doi.org/10.1039/C4RA06175F>
- [13] B. Lin, Y. Liu, L. Heng, J. Ni, J. Lin, L. Jiang, Effect of barium and potassium promoter on Co/CeO₂ catalysts in ammonia synthesis, *J. Rare Earths*, 2018, **36**, 703–707. <https://doi.org/10.1016/j.jre.2018.01.017>